Jurnal Kejuruteraan 33(4) 2021: 875-882
https://doi.org/10.17576/jkukm-2021-33(4)-10

Magnetic Resonance Imaging-Based Estimation of Knee Cartilage Thickness with MATLAB

Joyce Sia Sin Yin[a], Tan Tian Swee[a*], Khairil Amir bin Sayuti[b], Ahmad Tarmizi Musa[b], Azli Bin Yahya[a], Matthias Tiong Foh Thye[a], Sameen Ahmed Malik[a], Jahanzeb Sheikh[a], Jeremy Sia Yik Xian[a]

[a]Biomedical Engineering Programme,
School of Biomedical Engineering and Health Sciences,
Faculty of Engineering, Universiti Teknologi Malaysia, Malaysia
[b]Department of Radiology,
Universiti Sains Malaysia, Malaysia

**Corresponding author: tantswee@biomedical.utm.my*

Received 08 November 2020, Received in revised form 03 January 2021
Accepted 05 February 2021, Available online 30 November 2021

ABSTRACT

Detection of early knee osteoarthritis remains a driving force in the search for more promising quantitative assessment approaches. Apart from other conventional methods such as radiography, computed tomography, and sonography, magnetic resonance imaging has become more widely available and has made it essential to visualize the knee's entire anatomy. Biomarkers such as joint space narrowing, articular cartilage thickness, cartilage volume, cartilage surface curvature, lesion depth, and others are used to determine disease progression in non-invasive manner. In this research, a regional cartilage normal thickness approximation (RCN-ta) model was developed with MATLAB to enable rapid cartilage thickness assessment with a simple click. The model formulated was compared to the FDA-cleared software measurements. A reasonable range of 0.135-0.214 mm of root-mean-square error may be predicted from the model. With a high ICC > 0.975, the model was highly accurate and reproducible. A good agreement between the proposed model and the medically used software can be found with a high Pearson correlation of r > 0.90.

Keywords: Cartilage thickness; quantitative assessment; normal thickness; knee osteoarthritis; MATLAB

INTRODUCTION

Knee osteoarthritis (OA) is a frequently seen disease among the elderly and adults suffering from obesity or weakened anatomy due to serious knee injuries (Bijlsma et al. 2011). Evident pathological changes, such as cartilage erosion and regional thickness changes, can be seen in early illness and disease development. In Malaysia, the most common seen traditional diagnosis is joint-space narrowing (JSN) detection assisted with X-ray measurements due to its low cost and easy accessibility. However, this technique lacks statistical strength. OA signs are found only at a late stage of the disease, usually, in Kellgren and Lawrence (KL) grades 3 and 4, where the articular cartilage has undergone significant loss of its cartilaginous components and the development of osteophytes and sclerosis at the subchondral bone ends (Hayashi et al. 2012). Magnetic resonance imaging (MRI) is becoming more commonly available, making it a better measurement approach due to its ability to visualize the knee's entire joint structure (Eckstein et al. 2006).

Biomarkers such as JSN, articular cartilage thickness (ACT), cartilage volume, cartilage surface curvature, lesion depth, and others are used to determine disease progression in non-invasive manner. Among the tests, thickness calculation is the most direct quantitative approach to assist in diagnosis (Eckstein et al. 2006). 2-D thickness tests the distance between the articular cartilage and the ultrasonic knee bone (Steppacher et al. 2019). Some advanced 3-D knee cartilage reconstruction techniques allow for more accurate measurement of thickness perpendicular to the joint surface (Burgkart et al. 2001; Millington et al. 2007). Thickness estimation with 3-D reconstructed cartilage benefits in longitudinal studies while the 2-D calculation

is more based on disease diagnosis. On the contrary, a promising 3-D cartilage reconstruction needs intense attention on the part of experts to define cartilage boundaries using a snake model or an active shape family (Solloway et al. 1997). Recently, several interactive (H. S. Gan et al. 2014; Tang et al. 2006) and fully automated cartilage (Asghar et al. 2017; F. Liu et al. 2018; Yin et al. 2020) segmentation models have been proposed to replace the laborious marking process. Deep learning interferes with the development to replace human judgment on cartilage segmentation. As described above, a reliable database needs a high demand of experts' attention and time for labelling. The accuracy of automated whole knee cartilage segmentation remains insufficient to generate promising 3-D thickness computation.

To allow a prompt evaluation of ACT on the human knee MRI, we proposed a fast acquisition of average cartilage thickness with projections of cartilage edges on the Cartesian plane. The proposed model was built with the application MATLAB, where it had not been introduced in the database previously. In this paper, the related work on cartilage thickness computing was discussed in the next section, and the proposed thickness approximation system was presented in the methodology section; the results of the proposed model were contrasted with the measurements of the FDA-cleared ONIS-PACS application as discussed in the fourth section, the overall conclusion was made in the last part of the paper.

RELATED WORKS

Various methods are used to approximate cartilage thickness, including distance calculation using normal lines between intersection points on opposing cartilage boundaries, vertical distance or z-distance between boundaries, local thickness approximation, and field line projections, as shown in Figure 1 (Heuer et al. 2001; Maier et al. 2017). A small plane is fitted to the surrounding points to produce normal lines, the normal vector with an essential peculiar value of the covariance matrix is indicated. In most studies, the final thickness is then measured using Euclidean Distance Transform (EDT) and is proven to be the most appropriate distance approximation method (Desai & Hacihaliloglu, 2019; Dias, Vera Junn, Eunsung Mouradian, 2008; Graichen et al. 2003; Kauffmann et al. 2003; Y. Liu et al. 2020; Pakin et al. 2002; Tang et al. 2006). However, surface normal thickness computation is vulnerable to cartilage irregularities that causes outliers in the computed thickness map, as stated (Maier et al. 2017). The accuracy of the calculation can be enhanced by bringing further surrounding points into the own vector's formulation stage. Standard thickness computing can be easily influenced by noise, but current medical imaging contrast enhancement methods that provide resistance to noise amplification can overcome the problem (Asghar et al. 2017; H.-S. Gan et al. 2014; Sia et al. 2020). In addition to EDT, Eulerian partial differential equations (PDEs) were also proposed to quantify distance by integrating two solutions of Laplace equations obtained by the inner boundary and the outer boundary (Yezzi & Prince 2003).

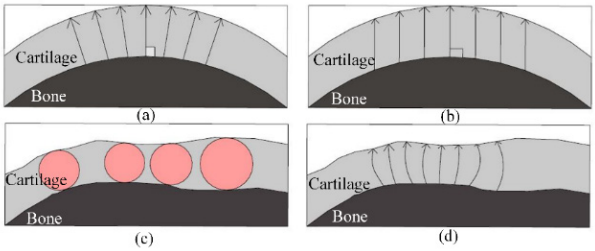

FIGURE 1. Four approaches in cartilage thickness computation with (a) surface normal (b) vertical lines (c) local thickness and (d) field lines.

Vertical distance approximation results in the most significant variance of measurements relative to other techniques. Among the methods of comparison, the technique produces the highest deviation of 7.06 percent from the calibration object, as stated (Heuer et al. 2001), showing the lack of relevance of the vertical distance approach in cartilage thickness measurement. For local thickness computation, the largest sphere is allocated to fit into the space given in the cartilage layer (Hildebrand & Rüegsegger 1997). Local thickness computation is vulnerable to error from the previous study. The underestimation in tibial cartilage thickness indicates that only a sphere with a maximum diameter will fit into irregular tibial cartilage (Shah et al. 2019). Field line (FL) thickness calculation is a newer method that suggests calculating the length of the FL emitted from one surface to another, provided that the two surfaces have different potentials. Unlike the normal line, FL is less susceptible to noise (Cao et al. 2015).

METHODOLOGY

KNEE MRI ACQUISITION AND SOFTWARE USED

20 MRI scans, including healthy knee (KL0) and diagnosed with disease progression (KL1 and KL2), were collected from the Osteoarthritis Initiative (OAI) database. Dual-echo steady-state (DESS) knee MRI with water excitation (we) is better positioned to visualize the human knee structure. Further information on the MRI protocols can be found on the following website: https:/nda.nih.gov/oai. The model

was fully developed with MATLAB version 2019a, and the data collected was analyzed with IBM SPSS Statistics 26.

REGIONAL CARTILAGE NORMAL THICKNESS APPROXIMATION (RCN-ta)

The proposed thickness computation model did not include a segmentation protocol, so the manual cartilage segmentations were carried out and checked by two expert observers. The segmentation results were then converted to binary images, resulting in bright pixels and dark pixels, representing cartilages and background respectively. As the average distance was determined between two opposing boundaries, the Sobel edge detector was slid through the image yielding the tibiofemoral cartilages' edges. Given that gradient g(m,n) where m and n are the pixel row and pixel column in an image I, can be defined as follows:

$$g_m = \begin{bmatrix} 1 & 0 & -1 \\ 2 & 0 & -2 \\ 1 & 0 & -1 \end{bmatrix} * I$$
$$g_n = \begin{bmatrix} 1 & 2 & -1 \\ 0 & 0 & 0 \\ -1 & -2 & -1 \end{bmatrix} * I \quad (1)$$

$$M(m,n) = \sqrt[2]{g_m(m,n)^2 + g_n(m,n)^2} \quad (2)$$

$$\theta(m,n) = tan^{-1}\left[\frac{g_n(m,n)}{g_m(m,n)}\right] \quad (3)$$

Sobel edge detectors apply both horizontal gradient operator g_m and vertical gradient approximator g_n. The gradient's direction can be approximated with the information obtained from the horizontal and vertical operators.

Notably that the input boundary image in Figure 2 was flipped upside down due to the difference in origin position. To allow the proper orientation of the pixel, the boundary pixels were mirrored with the centre line at the *y*-axis. The proposed RCN-ta model required a 'click' on any boundary point (p,q) as an input data cursor. Later, the point and its neighbouring pixels were convoluted with a 7×7 orientation detector to define its tangent direction, *O*.

$$O(p,q) = \begin{cases} horizontal\ line & , \quad if\ O = 0^{\circ} \\ vertical\ line & , \quad if\ O = \infty \\ line\ in\ quadrant\ I\ and\ III & , \quad if\ 0 < O \leq 90 \\ line\ in\ quadrant\ II\ and\ IV & , \quad if\ -90 < O \leq 0 \end{cases} \quad (4)$$

From equation (4), the tangent line orientation O_1 that falls in any of the four quadrants, the normal orientation O_2 can be obtained with the following equation:

$$\tan(O_2) = \frac{-1}{\tan(O_1)} \quad (5)$$

To generate a linear line to intersect the opposing boundary from the chosen point, the y-intersection was obtained with simple linear equation

$$c = q - \tan(O_2)p \quad (6)$$

A normal line was generated with the given linear equation as

$$y = \tan(O_2)\ x + c \quad (7)$$

For vertical tangent line, the resulting orientation is infinity. Therefore, there would be no linear estimation of the linear equation. The q coordinate was used to draw a straight line along the point with $y = q$. Similar to the horizontal tangent line, the resulting orientation is zero. The *p* coordinate was used to draw a straight line with $x = p$.

Surface normal is sensitive to surface irregularities present in the binary segmentation resulting from the previous stage. Improving the thickness measurements' precision, a bunch of normal lines near the clicked position may be emitted to their opposite borders. As a result, the average Euclidean pixel distance of the normal emitting lines was obtained instead of a single normal line. Since point (x, y) is the intersection point at opposing boundary and (x_o,y_o) is the normal line emission point, the single-pixel distance, the *P* equation can be computed as

$$P = \sqrt{(x - x_o)^2 + (y - y_o)^2} \quad (8)$$

With a preset distance magnitude of 3, the nearest boundary points emitted their respective n normal lines. The total pixel distance P_{total} of all normal lines and the average pixel distance P_{avg} are shown as follows:

$$P_{total} = \sum_{i=0}^{n} \sqrt{(x_i - x_{oi})^2 + (y_i - y_{oi})^2} \quad (9)$$

$$P_{avg} = \frac{P_{total}}{n} \quad (10)$$

The number of pixels, P_{avg} that laid within the intersections, was determined. The field of view (FOV) of the MRI slice was used to measure the actual cartilage thickness. Field of view of the MRI slice, *FOV* could be obtained by its pixel spacing, Δw. In this study, the MR images have a pixel width of 0.36458333 mm and an image size of *l*.

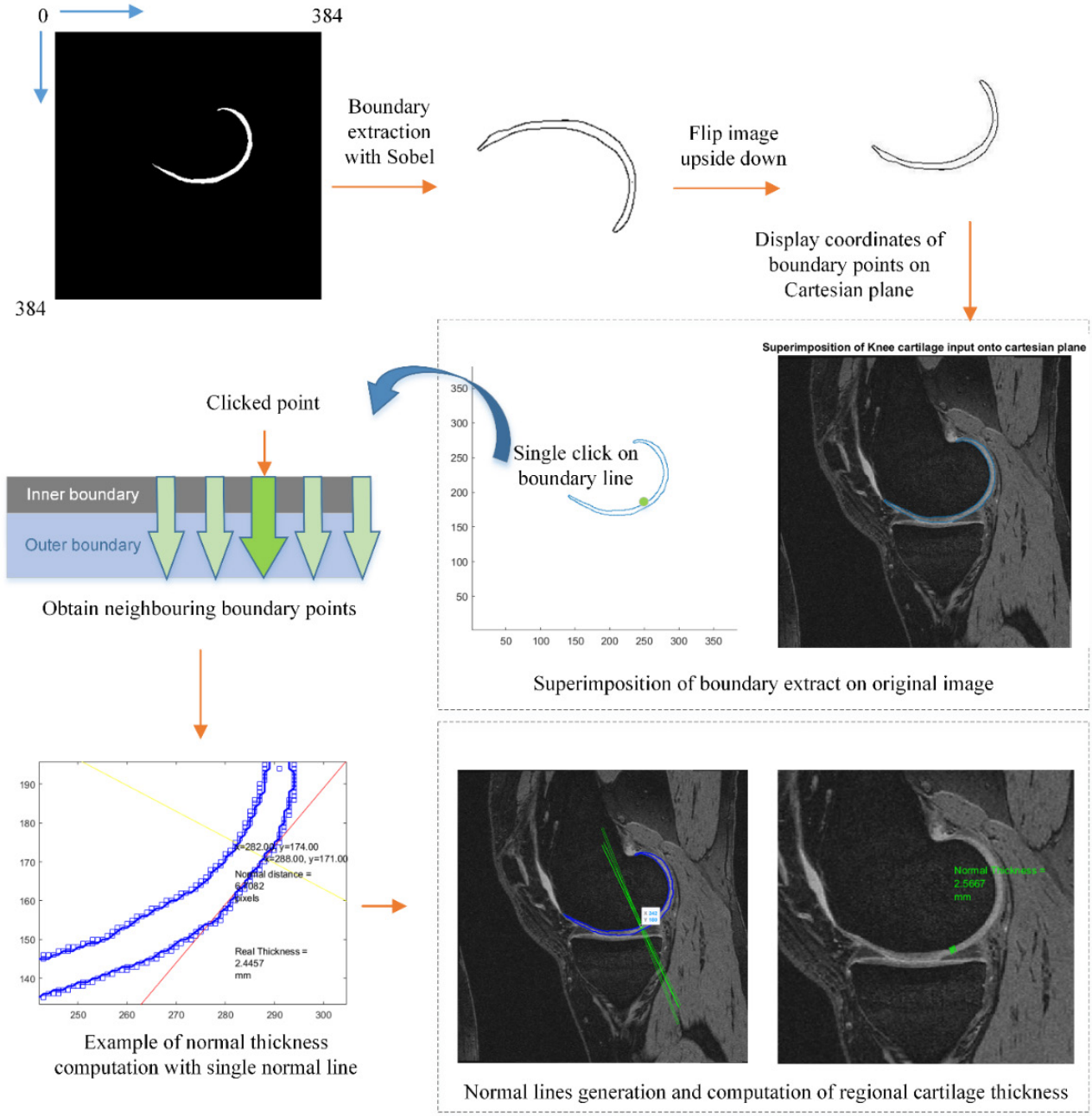

FIGURE 2. General illustration of thickness approximation process on Cartesian plane

$$FOV = \Delta w \times l \tag{11}$$

Given that the size of the image was 384 pixels, FOV calculated was 140mm. Thickness, T could be transformed with the following equation:

$$\frac{P_{avg}}{384} = \frac{T}{FOV}$$

$$T = \frac{P_{avg}}{384} \times FOV \tag{12}$$

Model Validation

The cartilage thickness estimation models discussed were validated with in-vitro disarticulated cartilage from removal surgery or a cadaver (Burgkart et al. 2001; Graichen et al. 2003; Millington et al. 2007) and in-vivo methods such as synthetic model (Kauffmann et al. 2003) and with calibrated measurement tools (Steppacher et al. 2019). In this analysis, the proposed model's measurements were compared with the FDA-cleared ONIS-PACS software at the six similar boundary locations (F_{CA},F_{CB},F_{CC},T_{CA},T_{CB},T_{CC}) as shown in Figure 4. The root-mean-square error (RMSE) and the maximum deviation between the measurements taken by the ONIS software and the proposed model were obtained. To detect the systemic error of the proposed

model, the Bland-Altman analysis (Steppacher et al. 2019) was performed by plotting the difference between the measurement instruments and their average thickness. Pearson coefficient and linear regression plot were used to check the association between the two measurements. The Pearson coefficient was rated as very weak for r<0.2, weak for 0.20-0.39, moderate for 0.40-0.59, strong for 0.60-0.79, and very strong for $r \geq 0.8$. In order to determine the reproducibility and reliability of the proposed model, intra-class correlation (*ICC*) was calculated. Given that *ICC* was graded as slight agreement at *ICC*<0.20, fair for 0.21-0.40, moderate for 0.41-0.60, substantial for 0.61-0.80, and good agreement for *ICC*>0.80.

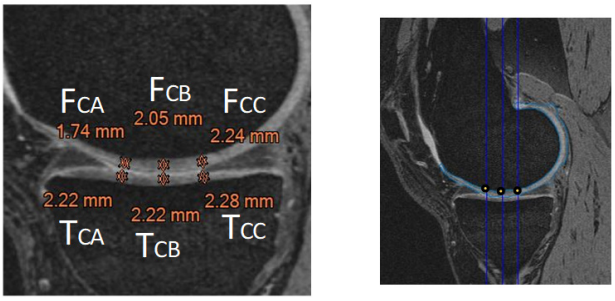

(a) (b)

FIGURE 4. A total of six measuring locations on weight-bearing regions. (a) Sample measurements with ONIS-PACS software. (b) Sample measurements with proposed model with vertical lines annotation to allow thickness computation at the same point as (a).

RESULTS AND DISCUSSIONS

To make a fair comparison between the proposed measuring tool and the ONIS software, the manual segmentations validated by two clinical radiologists were first fitted to the real cartilage edges with 3 to 5 iterations of the active contour using the Chan-Vese process. This stage was done to reduce the propensity of the image to be over-or under-segmented. From Table 1, the maximum observed errors and the root-mean-square error in the calculation of femoral cartilage thickness by Observer 2 is significantly higher than that of Observer 1. However, both Observer 1 and Observer 2 manual segmentations of tibial cartilage were subjected to higher error scores than femoral cartilage segmentation. The mean thickness of the 20 femoral and tibial cartilages were 2.190 *mm* and 2.215 *mm*, respectively. The RMS deviations recorded were 0.135 - 0.192 *mm* (observer 1) and 0.173 – 0.214 *mm* (observer 2) in femoral and tibial cartilages thickness measurements that fell in acceptable range of ±0.2-0.3 *mm* at weight-bearing regions (Koo et al. 2005).

Referring to the Bland-Altman plots in Figure 4, the nodes were uniformly and randomly distributed, suggesting no bias or major systematic error in the proposed thickness measurement model. The close relationship between the thickness measured from the proposed model and the ONIS program can be seen in Figure 5. High Pearson correlation scores were recorded between Observer 1 and validation set (r=0.973,p<0.01 for femoral cartilage; (r=0.909,p<0.01 for tibial cartilage). Similar to Observer 2, the Pearson correlation values between Observer 2 and the validation set were substantially high (r=0.954,p<0.01for femoral cartilage; r=0.911,p<0.01).

Based on *ICC* results in Table 2, the proposed model was highly reproducible and accurate with intra-observer values of 0.985 and 0.977 to measure femoral segment thickness, 0.953, and 0.951 for the tibial segment. The two observers' reliability ratings were 0.965 (femoral cartilage) and 0.940 (tibial cartilage).

The A-mode ultrasonic cartilage thickness measurements recorded in the past study can achieve a mean accuracy of 0.074 *mm* and 6% of the mean error (Ssteppacher et al. 2019). The promising accuracy of the control factors is restricted as follows: manual control of the angle of insonation (Steppacher et al. 2019), high spatial resolution (Graichen et al. 2003), suitable velocity (Millington et al. 2007) and other factors. In addition, the measurement's location retrieval is performed manually, which possibly examines different locations during the comparison stage. Although the proposed RCN-ta is prone to exhibit more significant RMS error when comparing exact position thickness measurements, it remains feasible to carry out a prompt knee OA assessment given the presence of specular noise and artifacts in the MRI. The proposed model is adaptable with variant cartilage segmentation tools to access the thickness of the cartilage. The precision of the cartilage thickness calculation relies strongly on the accuracy that can be tested with Dice similarity coefficient or Matthews correlation coefficient (MCC).

In future work, it is suggested that RCN-ta to be enhanced to enable the registration of medical images. For example, for the follow-up quantitative evaluation, the following session's MR slice, which demonstrates the most remarkable resemblance to the MR section of the previous clinical screening session, is selected. Retrospectively, the thickness of the cartilage can vary in the stage of disease development. Thus, the ability to monitor the thickness between similar slices at fixed locations helps to develop longitudinal disease pathogenesis studies and treatment progress.

TABLE 1. Maximum error and root mean square error between the manual segmented results collected through proposed thickness measurement model and ONIS software.

Examined Parts		Manual Segmentation	
		Observer 1	Observer 2
Femoral Cartilage	Mean thickness error/mm	0.002	0.060
	Max error/ mm	0.270	0.390
	RMS error/ mm	0.135	0.173
Tibial Cartilage	Mean thickness error/mm	0.078	0.104
	Max error / mm	0.350	0.330
	RMS error /mm	0.192	0.214

TABLE 2. Reproducibility and reliability test using ICC.

Parameter	Intra-observer 1	Intra-observer 2	Inter-Observer
FC Thickness	0.985(0.976 - 0.991)	0.977(0.961 – 0.986)	0.965(0.942 - 0.979)
TC Thickness	0.953(0.921 - 0.972)	0.951(0.918 – 0.971)	0.940(0.900 – 0.964)

* FC = femoral cartilage, TC = tibial cartilage
Values are expressed with mean of 95% confidence interval

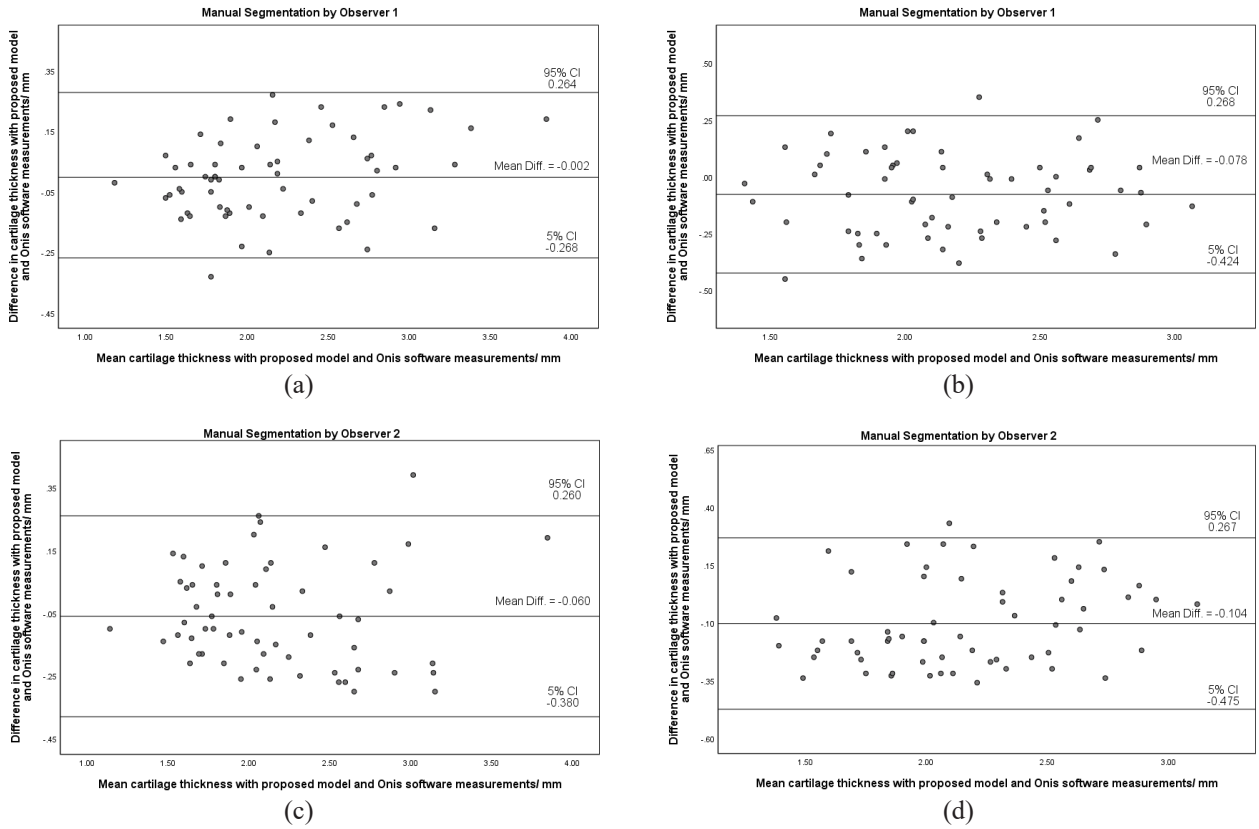

FIGURE 4. Bland-Altman plots of difference between the femoral cartilage thickness results obtained through the proposed model and ONIS software on manual segmentation (a) by observer 1 on femoral cartilage and (b) on tibial cartilage and (c) by observer 2 on femoral cartilage and (d) on tibial cartilage.

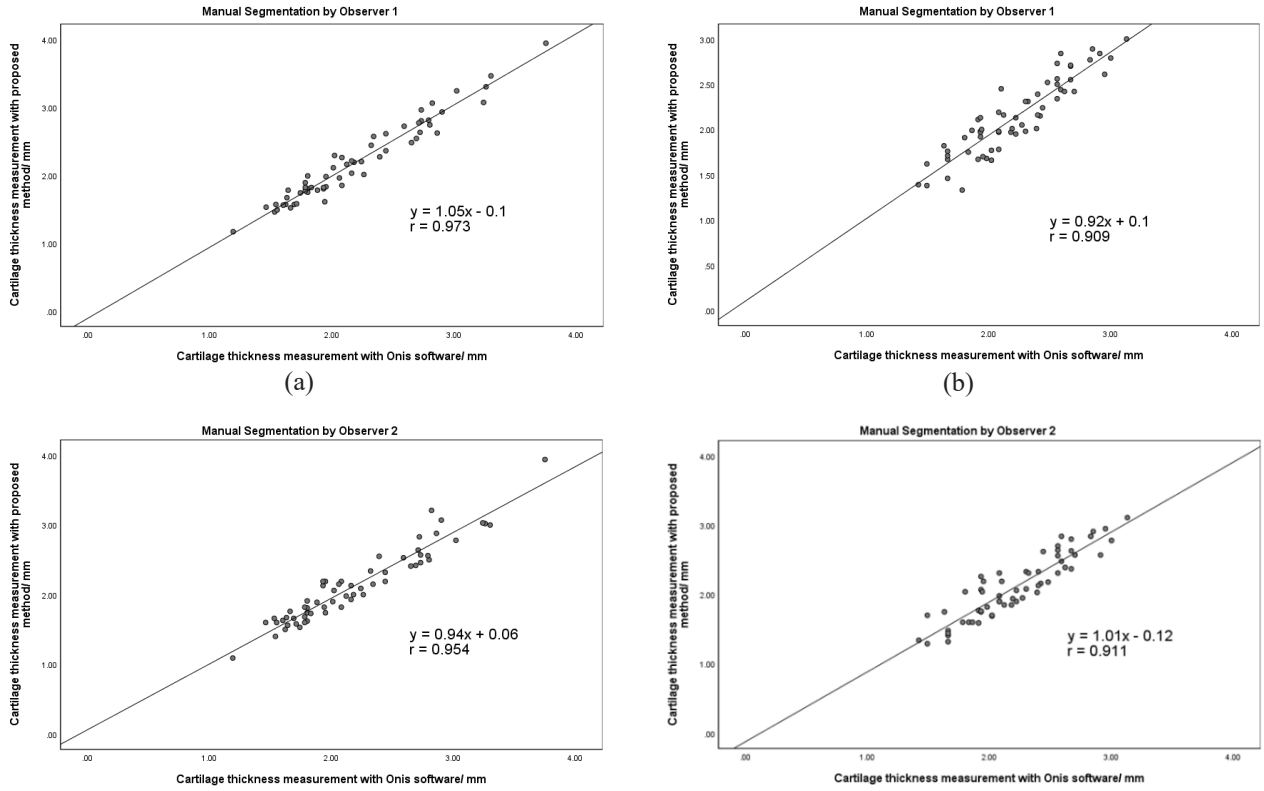

FIGURE 5. Linear regression plots cartilage thickness results obtained through the proposed model and ONIS software on manual segmentation by (a) observer 1 on femoral cartilage (b) on tibial cartilage (c) observer 2 on femoral cartilage and (d) on tibial cartilage.

CONCLUSION

Quantitative evaluation, such as cartilage thickness estimation, remains vital for access to disease progression and treatment effectiveness. The proposed RCN-ta model is tested with RMS error, intraclass correlation coefficient, systematic error detection with Bland-Altman analysis, and linear regression. A reasonable range of 0.135-0.214 *mm* RMS error could be expected from the model. With a high $ICC > 0.975$, the model is highly reliable and reproducible. A good agreement between the proposed model and the FDA-cleared ONIS-PACS program with a high Pearson correlation of $r > 0.90$ can be observed. The RCN-ta model allows for rapid cartilage evaluation. The registration feature is also encouraged to be applied to the proposed model to allow longitudinal follow-up evaluation.

ACKNOWLEDGEMENT

The authors would like to express their deepest appreciation to Universiti Teknologi Malaysia for their financial support under the grant Q.J130000.3051.01M61.

DECLARATION OF COMPETING INTEREST

None

REFERENCES

Asghar, K., Gilanie, G., Saddique, M., & Habib, Z. 2017. Automatic enhancement of digital images using cubic Bézier curve and Fourier transformation. *Malaysian Journal of Computer Science* 30(4): 300–310.

Bijlsma, J. W. J., Berenbaum, F., & Lafeber, F. P. J. G. 2011. Osteoarthritis: An update with relevance for clinical practice. *The Lancet* 377(9783): 2115–2126.

Burgkart, R., Glaser, C., Hyhlik-Dürr, A., Englmeier, K. H., Reiser, M., & Eckstein, F. 2001. Magnetic Resonance Imaging-Based Assessment of Cartilage Loss in Severe Osteoarthritis: Accuracy, Precision, and Diagnostic Value. *Arthritis and Rheumatism* 44(9): 2072–2077.

Cao, Q., Thawait, G., Gang, G. J., Zbijewski, W., Reigel, T., Brown, T., Corner, B., Demehri, S., & Siewerdsen, J. H. 2015. Characterization of 3D joint space morphology using an electrostatic model (with application to osteoarthritis). *Physics in Medicine and Biology* 60(3): 947–960.

Desai, P., & Hacihaliloglu, I. 2019. Knee-cartilage segmentation and thickness measurement from 2D ultrasound. *Journal of Imaging* 5(4): 1–19.

Dias, Vera Junn, Eunsung Mouradian, M. M. 2008. 基因的改变 NIH Public Access. *Bone* 23(1): 1–7.

Eckstein, F., Cicuttini, F., Raynauld, J.-P., Waterton, J. C., & Peterfy, C. 2006. Magnetic resonance imaging (MRI) of articular cartilage in knee osteoarthritis (OA): morphological assessment. *Osteoarthritis and Cartilage* 14: 46–75.

Gan, H.-S., Swee, T. T., Karim, A., Helmy, A., Sayuti, K. A., Kadir, A., Rafiq, M., Tham, W.-K., Wong, L.-X., & Chaudhary, K. T. 2014. Medical image visual appearance improvement using bihistogram bezier curve contrast enhancement: data from the osteoarthritis initiative. *The Scientific World Journal* 2014.

Gan, H. S., Tan, T. S., Karim, A. H. A., Sayuti, K. A., & Kadir, M. R. A. 2014. Interactive medical image segmentation with seed precomputation system: Data from the Osteoarthritis Initiative. *IECBES 2014, Conference Proceedings - 2014 IEEE Conference on Biomedical Engineering and Sciences: "Miri, Where Engineering in Medicine and Biology and Humanity Meet,"* December 2014 315–318.

Graichen, H., Jakob, J., von Eisenhart-Rothe, R., Englmeier, K. H., Reiser, M., & Eckstein, F. 2003. Validation of cartilage volume and thickness measurements in the human shoulder with quantitative magnetic resonance imaging. *Osteoarthritis and Cartilage* 11(7): 475–482.

Hayashi, D., Guermazi, A., & Roemer, F. W. 2012. *MRI of Osteoarthritis : The Challenges of De fi nition and Quanti fication* 1(212).

Heuer, F., Sommers, M., Reid, J. B., & Bottlang, M. 2001. Estimation of cartilage thickness from joint surface scans: Comparative analysis of computational methods. *ASME-PUBLICATIONS-BED* 50, 569–570.

Hildebrand, T., & Rüegsegger, P. 1997. A new method for the model-independent assessment of thickness in three-dimensional images. *Journal of Microscopy* 185(1): 67–75.

Kauffmann, C., Gravel, P., Godbout, B., Gravel, A., Beaudoin, G., Raynauld, J. P., Martel-Pelletier, J., Pelletier, J. P., & De Guise, J. A. 2003. Computer-aided method for quantification of cartilage thickness and volume changes using MRI: Validation study using a synthetic model. *IEEE Transactions on Biomedical Engineering* 50(8): 978–988.

Koo, S., Gold, G. E., & Andriacchi, T. P. 2005. Considerations in measuring cartilage thickness using MRI: Factors influencing reproducibility and accuracy. *Osteoarthritis and Cartilage* 13(9): 782–789.

Liu, F., Zhou, Z., Samsonov, A., Blankenbaker, D., Larison, W., Kanarek, A., Lian, K., Kambhampati, S., & Kijowski, R. 2018. Deep learning approach for evaluating knee MR images: achieving high diagnostic performance for cartilage lesion detection. *Radiology* 289(1): 160–169.

Liu, Y., City, I., Jin, D., City, I., Li, C., City, I., Janz, K. F., City, I., Burns, T. L., City, I., Torner, J. C., City, I., Levy, S. M., Dentistry, C., & City, I. 2020. *HHS Public Access* 61(7): 2057–2069.

Maier, J., Black, M., Bonaretti, S., Bier, B., Eskofier, B., Choi, J. H., Levenston, M., Gold, G., Fahrig, R., & Maier, A. 2017. Comparison of different approaches for measuring tibial cartilage thickness. *Journal of Integrative Bioinformatics* 14(2): 1–11.

Millington, S. A., Grabner, M., Wozelka, R., Anderson, D. D., Hurwitz, S. R., & Crandall, J. R. 2007. Quantification of ankle articular cartilage topography and thickness using a high resolution stereophotography system. *Osteoarthritis and Cartilage* 15(2): 205–211.

Pakin, S. K., Tamez-Pena, J. G., Totterman, S., & Parker, K. J. 2002. Segmentation, surface extraction, and thickness computation of articular cartilage. *Medical Imaging 2002: Image Processing* 4684(2002): 155.

Shah, R. F., Martinez, A. M., Pedoia, V., Majumdar, S., Vail, T. P., & Bini, S. A. 2019. Variation in the Thickness of Knee Cartilage. The Use of a Novel Machine Learning Algorithm for Cartilage Segmentation of Magnetic Resonance Images. *Journal of Arthroplasty* 34(10): 2210–2215.

Sia, J., Yin, S., Swee, T. T., Yahya, A. Bin, Tiong, M., Thye, F., Ling, K., Hiik, C., & Meng, L. K. 2020. *Prominent Region of Interest Contrast Enhancement for Knee MR Images : Data from the OAI* 32(3): 145–155.

Solloway, S., Hutchinson, C. E., Waterton, J. C., & Taylor, C. J. 1997. The use of active shape models for making thickness measurements of articular cartilage from MR images. *Magnetic Resonance in Medicine* 37(6): 943–952.

Steppacher, S. D., Hanke, M. S., Zurmühle, C. A., Haefeli, P. C., Klenke, F. M., & Tannast, M. 2019. Ultrasonic cartilage thickness measurement is accurate, reproducible, and reliable - Validation study using contrast-enhanced micro-CT. *Journal of Orthopaedic Surgery and Research* 14(1).

Tang, J., Millington, S., Acton, S. T., Crandall, J., & Hurwitz, S. 2006. Surface extraction and thickness measurement of the articular cartilage from MR images using directional gradient vector flow snakes. *IEEE Transactions on Biomedical Engineering* 53(5): 896–907.

Yezzi, A. J., & Prince, J. L. 2003. An Eulerian PDE Approach for Computing Tissue Thickness. *IEEE Transactions on Medical Imaging* 22(10): 1332–1339.

Yin, J. S. S., Swee, T. T., Thye, M. T. F., Meng, L. K., Hiik, K. L. C., Malik, S. A., & Xian, J. S. Y. 2020. K-means clustering in knee cartilage classification: Data from the OAI. *Indonesian Journal of Electrical Engineering and Informatics* 8(2): 320–330.